DIPODAL MOLECULAR DEVICE AS FLUORESCENT SENSOR FOR Na(I) DETECTION

Vijay Dangi [1], Minati Baral [1*], B. K. Kanungo [2]

[1] National Institute of Technology, Department of Chemistry, Kurukshetra, Haryana-136119, India
[2] Sant Longowal Institute of Engineering and Technology, Department of Chemistry, Longowal-148106, India; e-mail: minatibnitkkr@gmail.com

A novel dipodal fluorescent sensor, N^1,N^3-bis(2-(2,3,4-trihydroxybenzylidene)amino)ethylmalonamide (MEP), suitable for the practical measurement of sodium concentration has been successfully developed and characterized by several spectroscopic techniques. The design of the dipodal scaffold includes a central unit, spacer, and fluorophore moiety as structural key features. The fluorescence sensor MEP adopts a photoinduced electron transfer mechanism and shows excellent selectivity for Na(I) among other biologically and environmentally important metal ions, viz., Na(I), K(I), Al(III), Cr(III), Fe(III), Fe(II), Co(II), Ni(II), Cu(II), and Zn(II) in DMSO by demonstrating a remarkable enhancement in the fluorescence intensity from 345.5 to 705.5 a.u. at λ_{max} = 532.9 nm. The 1:2 binding stoichiometry between the ligand and Na(I) ion was confirmed by Stern–Volmer and Hill Plot. The association constant determined for the ligand with the sodium metal ion is found to be very high, 7.7×10^6 M^{-2}, which may be attributed to the trapping of sodium ions into the pseudo cavities of the ligand created by interaction of the ligand and sodium ions. The studies explore potential applications of the ligand for Na(I) ions detection in environmental and industrial applications.

Keywords: *dipodal chelator, pyrogallol, fluorescence, photoinduced electron transfer, sensor.*

ДИПОДАЛЬНЫЙ МОЛЕКУЛЯРНЫЙ ФЛУОРЕСЦЕНТНЫЙ СЕНСОР ДЛЯ ОБНАРУЖЕНИЯ Na(I)

V. Dangi [1], M. Baral [1*], B. K. Kanungo [2]

УДК 535.37

[1] Национальный технологический институт, Курукшетра, Харьяна-136119, Индия
[2] Инженерно-технологический институт Сант Лонговал, Лонговал-148106, Индия; e-mail: minatibnitkkr@gmail.com

(Поступила 22 июля 2019)

Разработан диподальный флуоресцентный датчик N^1,N^3-бис(2-(2,3,4-тригидроксибензилиден)амино)этилмалонамид (MEP), подходящий для практического измерения концентрации натрия, и охарактеризован несколькими спектроскопическими методами. Конструкция диподального каркаса включает в себя центральную единицу, спейсер и флуорофорную составляющую в качестве структурных ключевых особенностей. Датчик флуоресценции MEP использует механизм фотоиндуцированного переноса электронов и показывает превосходную селективность по Na(I) среди других ионов биологически и экологически важных металлов, а именно Na(I), K(I), Al(III), Cr(III), Fe(III), Fe(II), Co(II), Ni(II), Cu(II) и Zn(II) в ДМСО, демонстрируя заметное увеличение интенсивности флуоресценции с 345.5 до 705.5 отн. ед. при λ_{max} = 532.9 нм. Стехиометрия связывания 1:2 между лигандом и ионом Na(I) подтверждена зависимостями Штерна-Фольмера и Хилла. Константа ассоциации для лиганда с ионом металлического натрия очень высокая — 7.7×10^6 M^{-2}, что может быть связано с захватом ионов натрия в псевдополости лиганда, созданными взаимодействием лиганда и ионов натрия. Исследованы потенциальные применения лиганда для обнаружения ионов Na(I) в экологических и промышленных приложениях.

Ключевые слова: *диподальный хелатор, пирогаллол, флуоресценция, фотоиндуцированный перенос электронов, сенсор.*

Introduction. For physiological relevance, protons and metal ions such as sodium, potassium, calcium, and iron are the most popular targets for the development of new synthetic sensors. In the past decade, it is proved that sensors showed significant activity in the detection of biologically relevant metal ions and are well documented [1–3]. Many direct sensing schemes have been labeled for molecules in colorimetric and fluorescent chemosensors whose optical properties change upon binding with the cations [4–6]. These sensors need to show high selectivity for the metal ions over other interfering metal ions and to have a high association constant to enable metal chelation in the desired range. Sodium plays an important role in many physiological and pathological processes [7–10] and is known to be an essential alkali metal that is protuberant in extracellular fluids that controls the water level and electrolyte balance in the human body [11]. Any abnormality in its concentration may cause the risk of heart strokes or failure, diabetes, hyponatremia, and also kidney complications [12]. A large difference in the sodium concentration exists in between extracellular and intracellular compartments in animal cells. The range of concentration is 5–30 mM in intracellular sodium ions, and 100 mM in extracellular sodium ions, and these concentrations are maintained by their influx and efflux [13]. Also, sodium plays a major role in metallurgy; for example, excess of sodium, if present, can be precipitated out from the processing solution as sodium oxalates and considerably reduce the effectiveness of the overall processing operations in the Bayer process. Hence, it is very important to keep the concentration of sodium levels below some critical value to avoid such problems in the Bayer process. Further, leachable/extractable sodium oxide is a common contaminant that leaches out from medication items of glass and plastic materials. Therefore, the development of new sensors and devices for determining concentrations of ions is an important area of research [14, 15]. Keeping view of the above, a dipodal molecule N^1,N^3-bis(2-(2,3,4-trihydroxybenzylidene)amino)ethyl malonamide MEP (Scheme 1) was developed that carries two pyrogallol binding units joined to a malonate platform by an amide linkage through an ethylenediamine spacer. The presence of the pyrogallol unit in each arm of the dipodal ligand enables the possibility of detecting any metal-sensor interaction by changes in the emission spectrum.

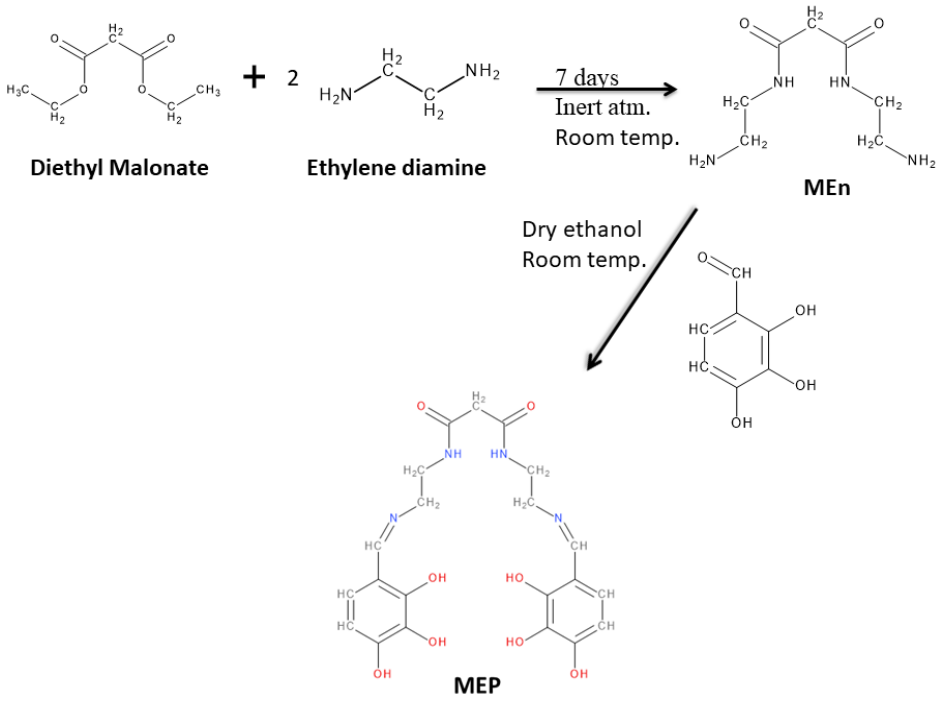

Scheme 1. Synthesis of dipodal ligand MEP.

Experimental. Sigma Aldrich chemicals were used for the synthesis without further purification. Ethanol, dichloromethane, diethyl ether, and DMSO were purchased from Loba Chemie, and the metal salts from Merck. The solutions were prepared in DMSO solvent. All the spectrophotometric and fluorescence studies were carried out in DMSO. Spectrophotometric studies were conducted on Evolution 201 Thermoscientific UV-Vis spectrophotometer, and the fluorescence spectra were recorded on Cary Eclipse fluorescence spectrophotometer with excitation and emission slit width of 5 mm and 10 mm, respectively, in a 10-mm quartz cuvettes.

Synthesis of MEn (intermediate compound). The intermediate product MEn was prepared from 10 g (0.0624 moles) of diethyl malonate by reacting it with a small excess of ethylenediamine (9.38 g, 0.156 moles). The mixture was stirred for 7 days at room temperature, which produced an off white precipitate of the condensed product. The excess of amine was removed by a rota-evaporator under reduced pressure, and the precipitate was washed several times with cold dry methanol, filtered, and dried in vacuum to produce MEn as a white powder with a yield of 76%. The compound is highly soluble in water. The decomposition temperature is 201–205°C. IR spectrum (KBr): $\nu_{(-C=O)}$ =1668 cm^{-1}, $\nu_{(-NH)}$ = 3290.56 cm^{-1}, and bending (-NH) = 1546 cm^{-1}.

Synthesis of MEP. To a 10 mL solution of MEn (0.5 g, 0.00266 moles) in absolute ethanol, 2,3,4-trihydroxybenzaldehyde (1.02349 g, 0.00664 moles) in 5 mL of ethanol was added dropwise with magnetic stirring in N_2 atmosphere at 45°C, and stirring was continued for 2 h. A bright yellow ppt. was obtained, which was filtered off, washed with cold ether, and dried in vacuum. The yield of the compound is 91.2% and the melting point is 178°C. ^{1}H NMR (DMSO-d_6, 400 MHz): δ 3.6 (t, 2H, OC-C**H$_2$**-CO), 3.1 (m, 4H, HN-C**H$_2$**-CH$_2$), 3.2 (m, 4H, HN-CH$_2$-C**H$_2$**), 3.4-3.5 (broad, s, 6H, Ar-O**H**), 6.5-8.1 (m, 4H, Ar**H),** 8.2 (s, 2H, CH=N), 9.7 (t, 2H, OC-N**H**-CH$_2$). ^{13}C NMR (DMSO-d_6, 400 MHz): δ 38.4 (HN-**C**H$_2$-CH$_2$), 54.42 (OC-**C**H$_2$-CO), 43.2 (CH$_2$-**C**H$_2$-NH), 106.7-122.9 (Ar**)**, 132.2-156.54 (Ar**C**-OH), 165.91 (**C**=N), 167 (O**C**-CH$_2$-**C**O). Mass spectrum (ESI-MS$^+$): $C_{23}H_{28}N_4O_6$: 460.44 (calc.), 463 (found, M+3).

Fluorescence studies. The photophysical properties of the ligand MEP were investigated in DMSO medium at 10^{-4} M concentration at room temperature. The electronic spectrum shows bands at λ_{max} = 310 and 410 nm. The emission spectrum of the ligand solution was recorded with an excitation at 410 nm with slit widths of 5 and 10 mm for excitation and emission, respectively, in a 10 mm quartz cell. The selectivity of ligand towards Na(I) metal ion out of a wide range of biologically and environmentally relevant metal ions was evaluated from the changes in the fluorescence intensity of the ligand upon addition of the metal ions. The association constant of the ligand with the metal ion was determined by B-H plot. The ligand and metal ions solutions in DMSO at concentration of 10^{-4} and 10^{-3} M, respectively, were used for the fluorimetric titration. The solutions were mixed thoroughly, and the spectra were recorded at the same excitation value (410 nm).

Stoichiometry determination for the ligand-metal complex. To determine the ligand and metal stoichiometry in the complex, the Stern-Volmer plot and Hill plot methods were used. The solutions were prepared in DMSO at 25°C, with the concentration of the ligand fixed at 50 μM; the concentration of Na(I) added to the ligand was varied from 0 to 300 μM. Fluorescence spectra were recorded at λ_{exc} = 410 nm, and the fluorescence intensity at λ_{max} = 532.9 nm was used for the calculations by using the Stern-Volmer equation derived for different stoichiometries of complexes:

$$I_0/I = 1 + K_{SV}\{\text{Na(I)}\}^n,$$

where I_0 is the fluorescence intensity of the ligand MEP, I is the fluorescence intensity in the presence of Na(I), n is stoichiometry of the complex, and K_{SV} is the Stern-Volmer constant.

Fluorescence lifetime measurements. The fluorescence intensity decay curves of the ligand only and in the presence of Na(I) metal ions were obtained by using Delta Flex TCSPC Lifetime Fluorimeter (Horiba) in DMSO medium at 10^{-4} M concentration. The fluorescence emission was registered at 532.9 nm upon excitation at 410 nm using a laser source with a pulse duration of ≈25 ps. The decay curves obtained were analyzed by the EZ Time program.

Potentiometric measurements. Protonation constants of the ligand and formation constants of its complex with Na(I) were determined by the potentiometric method. The titrations were carried out in a double wall glass jacketed titration flask at a constant temperature at (25 ± 1)°C. An Orion star-A111 Thermo Scientific pH meter with Ross Ultra pH/ATC glass electrode was used for the pH measurement. The electrode was calibrated by a classical method to read the pH. The ligand and Na(I) ions at a concentration 1×10^{-4} M were titrated against a standardized 0.095 M KOH solution to determine the formation constants. The solution was acidified to a pH of 2.5 using standardized 0.1 M HCl (1 mL) and the ionic strength was maintained with 0.1 M KCl solution. The data obtained from the titration were refined by the nonlinear least squares refinement program Hyperquad [16] to calculate the protonation and formation constants.

Spectrophotometric measurements. Absorption spectra were recorded on a Thermo Scientific Evolution 201 UV-Vis spectrophotometer using 1 cm path length at room temperature. The spectrophotometric titrations of the ligand and its complexation with sodium ions were carried out under similar conditions as for potentiometric titrations at a concentration 1×10^{-4} M in DMSO for both ligand and metal ions. After recor-

ding the spectra of the solution at a particular pH, the aliquot was transferred back to the titration flask carefully each time so that the volume loss is negligible. The protonation of the ligand and formation constants of the sodium metal complex were evaluated by using a nonlinear least square fitting program using the computer software HYPSPEC [17].

Result and discussion. *Synthesis and structural characterization of MEP.* To examine the effect of flexibility on the binding efficiencies of the ligand, a suitable spacer was incorporated in the dipodal structural framework, and the ligand was designed under three domains: central unit (diethyl malonate), spacer (ethylenediamine), and binding units (pyrogallol). For this, we attached the binding unit to the central unit by the spacers through an amide (-NH-CO-) and imine (-NH=C-) linkage. The synthesis of dipodal MEP follows a two-steps reaction (nucleophilic substitution and condensation), as shown in Scheme 1. In the first step of the reaction, diethyl malonate and ethylenediamine were reacted to give a water-soluble white intermediate product MEn through a nucleophilic substitution reaction. The intermediate product was found to be moisture sensitive on exposure to air. The peaks in the IR spectrum validated the insertion of the spacer group (ethylene) through an amide linkage. In the second step, two binding units (pyrogallol) were incorporated into the intermediate via a condensation reaction. For this, the reaction between the intermediate compound (MEn) and 2,3,4-trihydroxybenzaldehyde was carried out at room temperature in dry ethanol to yield 91.2% of Schiff base compound MEP. The compound has a sharp melting point at 178°C and is completely soluble in DMSO and partially soluble in water. Characterization of the compound by ^{1}H NMR, ^{13}C NMR, IR, and mass spectroscopic techniques establishes the formulation of the dipodal ligand.

FT-IR analysis. The FT-IR spectrum of MEP was recorded on a Shimadzu FT-IR spectrometer in the mid-IR range (4000–400 cm^{-1}) as KBr pellet in the transmission mode. The presence of the amide linkage due to ester and amine condensation was confirmed by the appearance of a characteristic sharp peak for $\nu_{(-C=O)}$ at 1668 cm^{-1}. The bands due to $\nu_{(-NH)}$ and $\delta_{(-CONH-)}$ appeared at 3290 and 1546 cm^{-1}, respectively, further establishing the presence of the amide group in the intermediate molecule. Formation of an azomethine (-N=CH-) group due to condensation of the intermediate amine and 2,3,4-trihydroxybenzaldehyde can be confirmed from the peak at 1639 cm^{-1}, which is attributed to $\nu_{(-C=N)}$ vibration. It is documented that if the nitrogen atom of the C=N bond has a more polar character, the transmission is found in the region 1659–1510 cm^{-1}, whereas for normal C=N it is expected in the range 1680–1650 cm^{-1} [18, 19]. The vibrational frequency of –OH group of phenols is reported in the range of 3550–3200 cm^{-1} [20]. Here, the broad band at 3290 cm^{-1} is due to $\nu_{(-OH)}$ stretching for the aromatic hydroxyl group, which is merged with the –NH stretching vibrations. Moreover, $\nu_{(-CH)}$ of an aromatic ring can be confirmed by the appearance of the characteristic peak at 3072 cm^{-1}.

^{1}H NMR analysis. The chemical environment of different protons present in the ligand was determined through the ^{1}H NMR spectrum recorded in deuterated DMSO. In total, nine protons of a different kind were found in the ^{1}H NMR spectrum, as expected in the case of the ligand. Out of three methylene (-CH_2-) groups, the most deshielded protons are for the active methylene group of the central unit due to the presence of two adjacent carbonyl moieties appearing as singlets (2H) at 3.6 ppm whereas, and the triplets at 3.2 and 3.1 ppm are attributed to the methylene groups attached to the imine group and amide group, respectively. The imine protons (-C**H**=N-) appeared as a doublet (2H) at 8.2 ppm, and the multiplet in the range of 6.2–7.0 ppm was attributed to the aromatic protons. Amide protons (-CO-N**H**-) were observed at 9.7 ppm (t, 2H), and the broad peak (s, 6H) observed at 3.4-3.5 ppm is due to six hydroxyl groups (-OH) attached to the aromatic rings.

^{13}C NMR analysis. The carbon skeleton of the ligand was established by the ^{13}C NMR spectrum taken in DMSO-d_6. The peaks obtained in the range of 106.7–122.7 ppm correspond to the aromatic carbons, and the chemical shift at 165.9 ppm is attributed to the carbon of –N=**C**H groups. Peaks obtained in the range 132.2–156.54 ppm are for the aromatic carbons (Ar**C**-OH) at which hydroxyl groups are attached. The peaks at 38.4 and 43.2, are attributed to two methylene groups of the spacers, whereas the –**C**H_2- group of the central unit (malonate) is the most deshielded one among all the methylene groups because it is flanked by two electron-withdrawing groups (-CO-) in the vicinity, which appeared at 54.42 ppm.

Mass analysis. The molecular mass of the ligand was calculated by ESI-MS technique. The mass spectrum of MEP showed a parent molecular peak (*m*/*z*) at 463.3 (calc. 460.4), which can be assigned to the M+3 peak. The peak at 443 fits the formulation of $C_{21}H_{23}N_4O_7$, which can be due to the loss of one hydroxyl group from the pendant arm followed by further loss of 5[O] and -C_5H giving rise to *m*/*z* at 302.59. The fragmented base peak at 274.57 (calc. 272.57), corresponding to the formation of $C_{16}H_{24}N_4$, might be

due to the loss of one binding unit (pyrogallol) with the rest of all the hydroxyl groups and carbonyl oxygens from the parent compound.

Photophysical studies. The electronic spectrum of the ligand recorded in 10^{-4} M DMSO showed bands at λ_{max} = 310 nm ($\varepsilon = 1.19 \cdot 10^4$ L/(mol · cm)) and at 410 nm ($\varepsilon = 0.42 \cdot 10^4$ L/(mol · cm)) corresponding to $\pi \rightarrow \pi^*$ and $n \rightarrow \pi^*$ transitions having energies 4.002 and 3.026 eV, respectively. A significant hypochromic shift in the absorbance of the ligand was observed along with a prominent hypsochromic shift upon the addition of 10^{-4} M Na^+ ions to the ligand solution. The band shift at 310 to 282.6 nm ($\varepsilon = 3.315 \cdot 10^4$ L/(mol · cm) and another from 410 to 342.4 nm ($\varepsilon = 3.24 \cdot 10^4$ L/(mol · cm)) clearly specifies the interaction of the ligand with the sodium metal ion, as depicted in Fig. 1. The molecular modeling studies were also carried out at the DFT level to confirm the assignments and to compare the experimental electronic spectra. The molecular orbitals corresponding to the transitions calculated from the DFT are presented on the right side of Fig. 1. The hybrid functional B3LYP with 6-311G** basis set were used for the ligand, whereas the LANL2DZ basis set was used for the calculation of the complex.

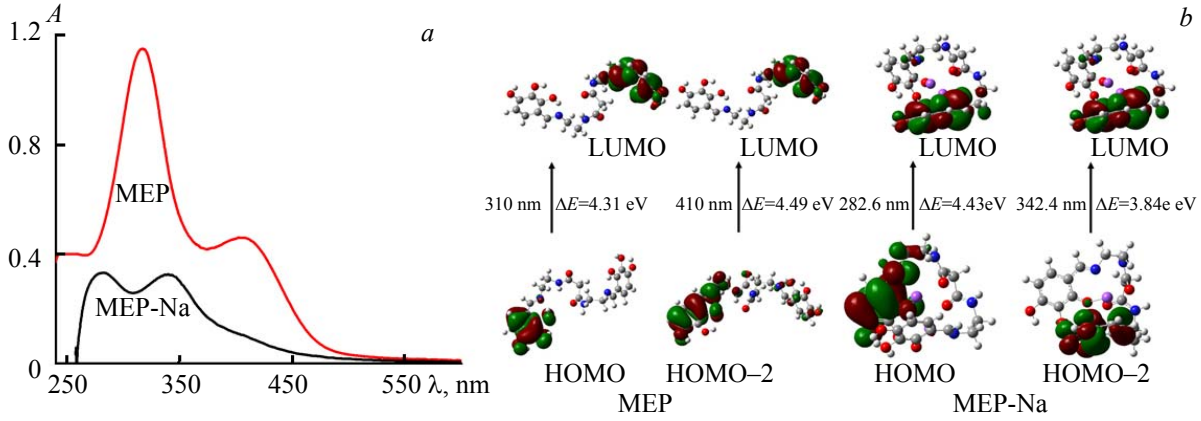

Fig. 1. Electronic spectra of the ligand in the presence of Na(I) in DMSO at concentration 10^{-4} M at 25°C (a). Molecular orbitals corresponding to the transitions MEP-Na and MEP calculated by DFT method using B3LYP/6-311G** for the ligand and B3LYP/LANL2DZ for the complex (b).

The emission spectrum of MEP recorded in DMSO medium at 10^{-4} M concentration upon excitation at λ_{exc} = 410 nm showed a band at 532.9 nm with intensity 345.5 a.u.. Further, the fluorescence behavior of the ligand was investigated in the presence of various monovalent, divalent, and trivalent metal ions, viz., Na(I), K(I), Al(III), Cr(III), Fe(III), Fe(II), Co(II), Ni(II), Cu(II), and Zn(II), in the same medium. Among all the metal ions chosen, a remarkable change in the fluorescence emission of the ligand was detected in the presence of Na(I), which exhibited a large enhancement of about 360 a.u. as shown in Fig. 2.

Except for cobalt and zinc metal ions, no other metal ions could bring any noticeable change to the ligand's emission spectrum, as depicted in Table 1, which shows the ratio of the fluorescence intensity of the ligand over the intensity of the emission in the presence of the metal ions. However, further study

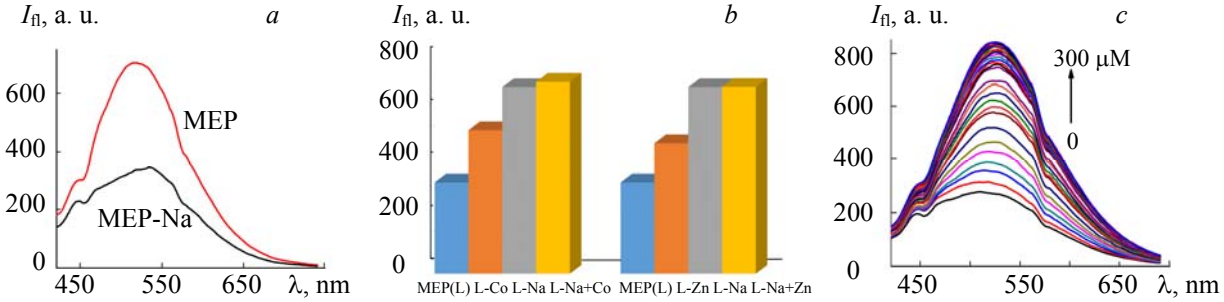

Fig. 2. Fluorescence spectra of MEP in the presence of Na^+ ion at conc. 10^{-4} M at 25°C (a), non-interference of the other interfering metal ions (Co^{+2} and Zn^{+2}) on the fluorescence intensity of MEP-Na in 10^{-4} DMSO (b), and changes in fluorescent spectra of MEP on successive addition of Na(I) (0–300 μM) in DMSO (c).

TABLE 1. Ratio of Fluorescence Intensities of the Ligand Upon Addition of a Particular Metal Ion in DMSO at Concentration 10^{-4} at 25°C

Metal ions	I_0/I
MEP (L)	1
L-Na(I)	**2.04**
L-K(I)	1.21
L-Al(III)	0.54
L-Cr(III)	0.75
L-Fe(III)	0.47
L-Fe(II)	0.78
L-Co(II)	1.54
L-Ni(II)	1.09
L-Cu(II)	1.22
L-Zn(II)	1.44

revealed that the change in the fluorescence emission intensity of MEP-Na is negligible in the presence of both cobalt and zinc ions (Fig. 2), which indicates non-interference of the metal ions (cobalt and zinc) on the ligand's high selectivity for the detection of sodium metal ions.

To gain an insight into the effect of concentration on the ligand's selectivity for Na(I) ion, a titration was performed. In the successive addition of Na(I) of concentration 5–300 μM to the solution of MEP (10^{-4} M), a concentration-dependent enhancement was observed, as depicted in Fig. 2. The plot of normalized intensity against the logarithm of concentration shown in Fig. 3a illustrates good linearity in the range 5–100 μM. The fluorescence detection limit (LOD) of MEP for Na^+ was obtained from the calibration curve of the experimental data. The plot of change in fluorescence intensity versus [Na^+] is linear, and the regression coefficient was found to be 0.99845, as shown in Fig. 3. The limit of detection for Na(I) was calculated as $1.98 \cdot 10^{-4}$ by using the relation 3σ/K [19].

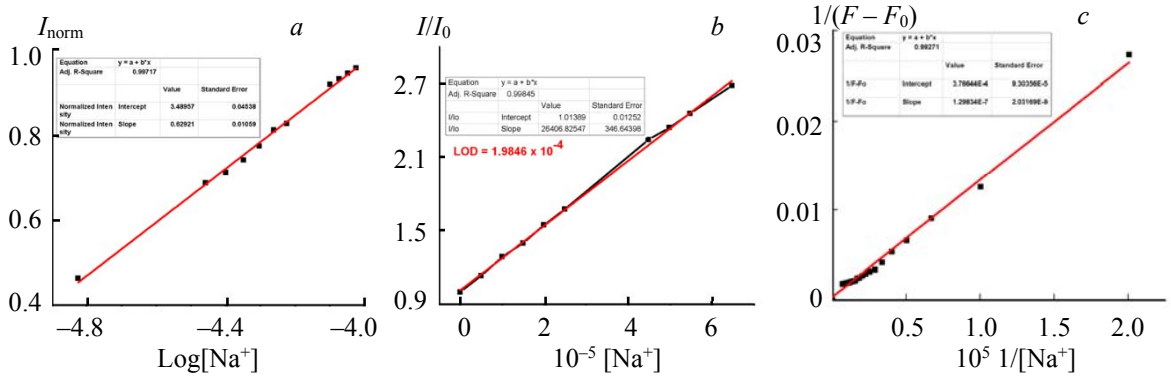

Fig. 3. a) Plot of normalized intensity against concentration of Na(I) (5–100 μM); b) Plot of fluorescence intensity ratio against concentration of Na(I) for determining the limit of detection (LOD); c) B-H Plot to calculate association constant MEP-Na(I).

Practical use of many fluorophore compounds working on the PET (photoinduced electron transfer) mechanism has already been demonstrated [21–23]. An imino-phenol proton transfer (tautomerism) occurring in the excited state through the interaction of hydrogen (of –OH) and nitrogen (of imine) favors the PET mechanism where the free lone electron pair of nitrogen acts as a donor moiety and –OH of the phenol (here pyrogallol) moiety acts as an acceptor group. In the present case, due to the formation of a very weak interaction between imine –N and hydrogen (–OH), a weak PET mechanism is observed, which leads to fluorescence with intensity ~345.5 a.u. However, in the presence of Na(I) ion, the interaction of Na(I) with imine (–N) becomes prominent, and the free electron pair of the nitrogen atom is partially shifted towards metal ions, leading to cessation of the PET mechanism with rise in fluorescence intensity [24, 25]. The sodium ion can be considered as bonded to the imine nitrogen and deprotonated oxygen of the pyrogallol binding unit as shown in Fig. 4. The PET on-off mechanism is shown in Fig. 5.

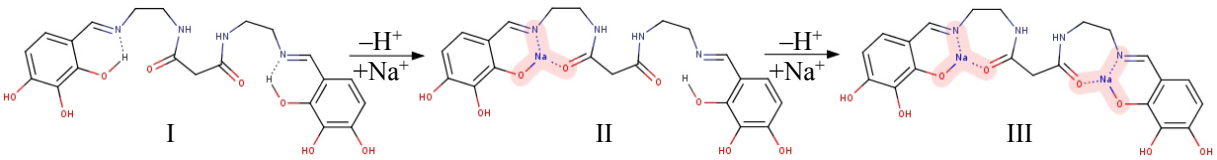

Fig. 4. Formation of two sodium ions in the ligand MEP. Weak interaction between lone pair of N and H due to hydrogen bonding, amounting toweak fluorescence. Strong fluorescence (III) due to N-lone pair-Na(I) interaction.

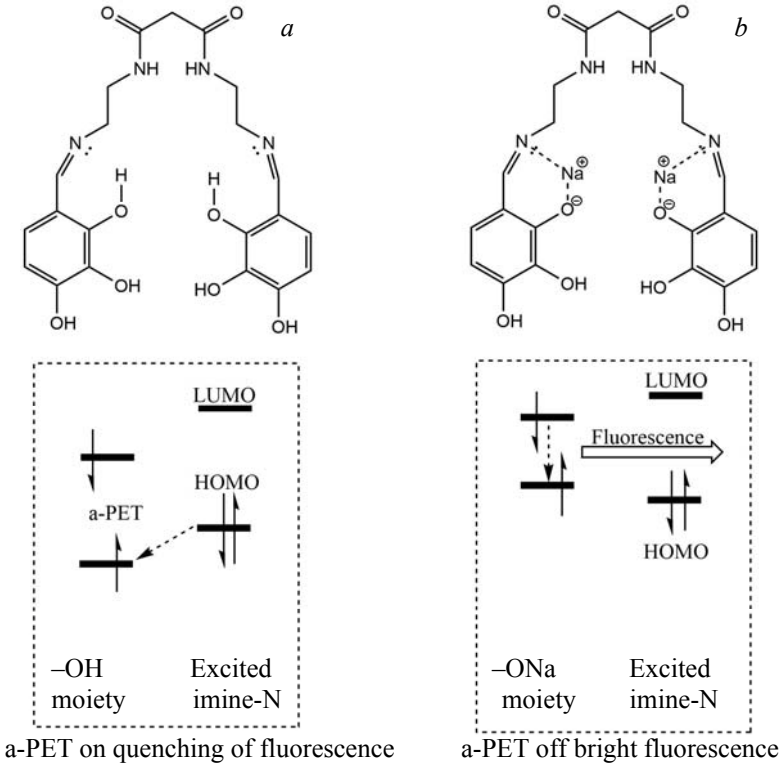

Fig. 5. Proposed PET mechanism: a restricted "PET-on" mechanism in MEP molecule (a) due to weak N-H interaction and "PET-off" mechanism in Na-MEP complex (b).

In order to get a clear picture of the process, DFT studies were undertaken for the ligand as well as the Na-ligand complex. The O-H and N…H bond distance in the DFT optimized structure of the ligand were found to be 0.7 and 1.8 Å, respectively, indicating the existence of a very weak interaction between the imine N and H of the ortho –OH of the pyrogallol unit. Interestingly, in the optimized structure of the Na-ligand complex, it is observed that the sodium ion is captured in a pseudo-cavity generated by an oxygen (O^1) of the ortho –OH, N of imine and another oxygen (O^2) of the amide group. The Na-O^1, Na-N, and Na-O^2 bond distances were found to be 2.13, 2.41, and 2.26 Å, respectively. The optimized geometry of the ligand and its sodium complex are shown in Fig 6. The existence of such pseudo-cavities for some other Na-ligand complexes has been documented [26]. The Na-O and Na-N bond distances are comparable with the Na-aza-macrocycle complexes (Na-O = 2.313 Å, Na-N = 2.438 Å) [27]. Since two pseudo-cavities are generated in the metal-ligand complexes, the experimental observation of formation of Na_2L type complex can be justified.

The Benesi-Hildebrand plot [28], a plot of $1/(F - F_0)$ vs $1/[Na^+]$ (where F_0 is the initial intensity and F is the final intensity of fluorescence emission), was obtained by continuous addition of Na(I) of concentration 10^{-3} M to the solution of ligand MEP of concentration 10^{-4} M; a concentration-dependent enhancement effect was observed that shows good linearity, R^2= 0.9927 (Fig. 3c). From the plot, we get the intercept and slope values which are as follows: intercept $1/(F_{max} - F_0) = 3.766 \times 10^{-4}$, and slope $1/K_a = 1.298 \times 10^{-7}$.

By inverting the slope, we calculate the association constant K_a. The association constant K_a of the complex calculated from the B-H plot by using the above equation was found to be $7.7 \cdot 10^6$ M^{-1}. By using the B-H plot we found that the Na(I) is bound with the ligand with a large association constant, and this can have potential applications in biological and environmental samples [27–29]. A comparison of association constants of sodium ions with the other reported ligands is shown in Table 2, which confirms that the MEP ligand is a potential chelator for the sodium ions.

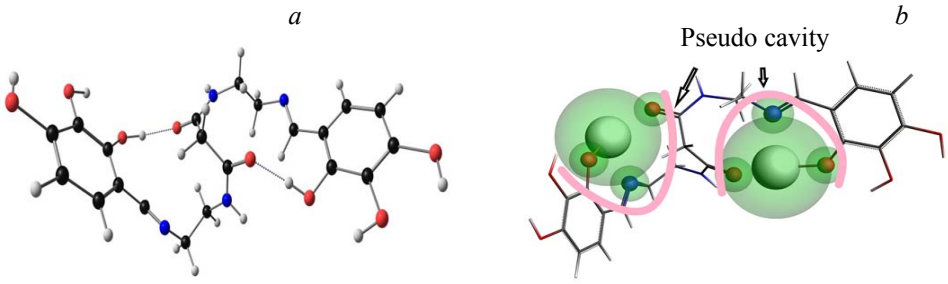

Fig. 6. DFT optimized structures of the ligand MEP (a) and Na-MEP complex (b). Interaction of Na(I) ions with MEP creates pseudo-cavity.

TABLE 2. Comparison of Association Constants of MEP and Other Reported Ligands with Na(I) ions

Ligands	Association Constants
Biginelli based ONPs [29]	7.9×10^4 M^{-1}
Pyrene unit Compound 39 [24]	1.1×10^4 M^{-1}
TFP [30]	2×10^4 M^{-1}
CPZ [30]	3.6×10^4 M^{-1}
BSA- cromolyn sodium [31]	2.7×10^4 M^{-1}
BSA- sodium warfarin [32]	4.9×10^4 M^{-1}
MEP	**7.7×10^6 M^{-2}**

We used the equation

$$\frac{1}{F - F_0} = \frac{1}{K_a(F_{\max} - F_0)[\mathrm{Na}^+]} + \frac{1}{F_{\max} - F_0}.$$

The PET quenching phenomenon and binding stoichiometry of the ligand MEP in the presence of Na(I) ions were further evaluated by the Stern-Volmer equation [33]. The Stern-Volmer plot, a plot of I_0/I vs $[Na^+]$ (where I_0 is the fluorescence intensity of the ligand and I is the fluorescence intensity of the ligand in the presence of metal ion, i.e., $[Na^+]$), was obtained by continuous addition of Na(I) of 10^{-3} M concentration to the ligand solution of the same concentration. When $n = 2$ in the equation $I_0/I = 1 + K_{SV}\{\mathrm{Na(I)}\}^n$, the plot gave a straight line with an excellent fit with $R^2 = 0.953$ (Fig. 7a), which confirmed the 1:2 stoichiometry of the ligand and metal interaction in forming the complex. The same stoichiometry was also confirmed from the Hill Plot presented in Fig. 7b. It was observed that after addition of two equivalents of Na(I) metal ions to the ligand solution, the excess of the metal ions added remained unbound in the solution, which can be seen by the attainment of saturation in the curve beyond a concentration of 1×10^{-4} M of metal ions, thus establishing the stoichiometry of the complex as 1:2.

The decay of the fluorescence intensities of the ligand MEP in the presence of Na(I) was also studied. The ligand fluorescence emission was shown to be at 532.9 nm when excited at 410 nm. The approximations given by the two exponentials gave χ^2 values from 14.63–1.53 for the ligand and 10.34–1.36 for the MEP-Na(I) complex. The average decay time τ was calculated using a Horiba TCSPC lifetime fluorimeter by employing the following equation [34]:

$$\langle\tau\rangle = (\sum A_i\tau_i^2)/(\sum A_i\tau_i),$$

where τ are the lifetimes of the components of the approximated decay curves; A is the corresponding relative amplitudes. The average decay time τ with their confidence interval of the ligand MEP is 0.31±0.0001 ns, and in the presence of Na(I) it is 0.32±0.0001 ns. The values of lifetimes and relative amplitudes with their pre-exponential factors are tabulated in Table 3. The relative amplitude of the ligand MEP increased from

81 to 83% on adding Na(I) ions in the ligand, indicating the binding of Na(I) ions with the ligand. It should be noted that more intense decay of the ligand may exist in the presence of Na(I). Nonetheless, the Na(I) dependent amplitudes and pre-exponential factors of the two decay times provide an explanation of why the fluorescence intensity or decay time increased in the presence of Na(I) ions.

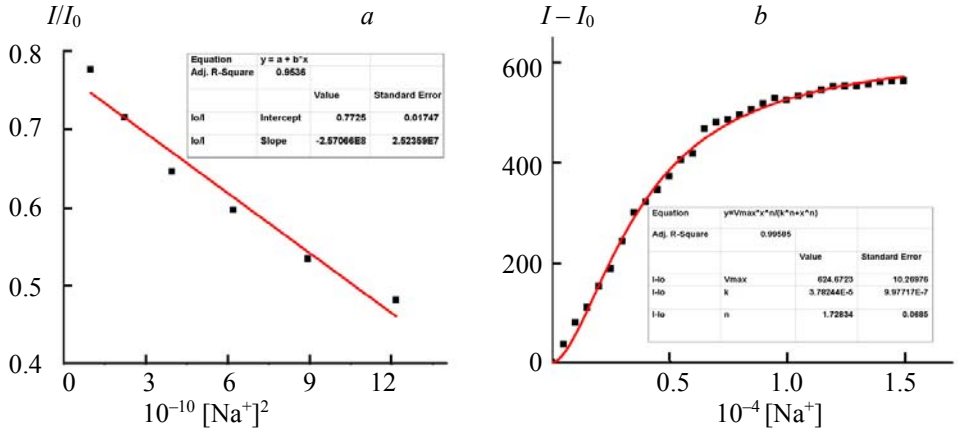

Fig. 7. a) Linear Stern-Volmer plot for the enhance of MEP in the presence of Na(I); b) Hill plot for the MEP in the presence of Na(I).

TABLE 3. Lifetimes, Relative Amplitudes, Pre-exponential Factors, and Average Lifetime of the Ligand MEP in the Presence of Na(I) Ions

Compound	Lifetimes, ns		Relative amplitudes, %		Pre-exponential factors		Average lifetime with CI, ns
	τ_1	τ_2	A_1	A_2	α_1	α_2	T
MEP	4.24	0.26	18.74	81.26	–0.01	0.99	0.31±0.0001
MEP-Na	4.18	0.27	16.97	83.03	–0.01	0.99	0.32±0.0001

Ligand protonation and metal binding constants. The protonation constant of the ligand MEP and the formation constant of the Na(I) metal complex were calculated by both potentiometric and spectrophotometric methods. The potentiometric titrations were carried out by adding an excess measured amount of standard HCl to the ligand and then titrating it against standard KOH at μ = 0.1 M KCl and (25±1)°C in 99:1 water: DMSO mixture in the pH range 2–11 since turbidity occurred after pH 11. The potentiometric titration curve for the ligand analyzed by using the program Hyperquad 2008 gave the best fit for the six protonation constants, along with the two hydrolysis species for the imine linkage in the ligand, as proposed by the equation

$$LH_{n-1} + H \rightleftharpoons LH_n, \quad K_{1n} = [LH_n]/[LH_{n-1}][H].$$

Potentiometric titration of MEP with Na(I) ion was carried out in 1:2 metal-ligand molar ratios at μ = 0.1 M KCl and (25±1)°C in a highly aqueous medium (99:1 water:DMSO mixture). The deviation of the Na-L potentiometric curve from the free ligand curve confirms the formation of the metal complex at a lower pH. As turbidity occurred at higher pH, data up to pH 11 were used for the calculation. A set of possible species formed during complexation was established, and the best-fit model was obtained when NaL and Na_2L species were considered in the calculation. By using the Hyperquad 2008 program, the overall stability constants (log β) of the species were calculated, as shown in Table 4.

The absorption spectra of the ligand were recorded in the pH range of 2–11 from 240 to 600 nm, as shown in Fig. 8a. There is no apparent change in the absorption spectra from pH 2–4 but, with increase in pH, the absorption bands showed a bathochromic shift from 290 to 317 nm (assigned to $\pi \rightarrow \pi^*$) and 400 to 410 nm (assigned to $n \rightarrow \pi^*$) with a concomitant increase in the absorbance intensity, giving rise to three isobestic points. Six protonation constants, of which four are related to –OH pyrogallol, can be determined for the ligand for pyrogallol, which is the only chromophoric group present in the ligand that shows spectral changes.

TABLE 4. Protonation and Formation Constants (logβ) of MEP at 25±1°C and μ = 0.1 M KCl (A = potentiometry and B = spectrophotometry)

Equilibrium	logβ		Protonation Sites
	A	B	
$LH_3 + H \rightleftharpoons LH_4$	13.45	13.42 ± 0.03	(–OH, meta)
$LH_2 + H \rightleftharpoons LH_3$	12.36	12.38 ± 0.02	(–OH, meta)
$LH + H \rightleftharpoons LH_2$	10.87	10.85 ± 0.02	(–OH, ortho)
$L + H \rightleftharpoons LH$	8.78	8.77 ± 0.01	(–OH, ortho)
$LH_{-1} + H \rightleftharpoons L$	4.12	4.13 ± 0.01	(–NH, imine)
$LH_{-2} + H \rightleftharpoons LH_{-1}$	1.42	1.42 ± 0.00	(–NH, imine)
$LH_{-3} + H \rightleftharpoons LH_{-2}$	–0.24	–0.24 ± 0.00	(hydrolysis)
$LH_{-4} + H \rightleftharpoons LH_{-3}$	–1.56	–1.57 ± 0.01	(hydrolysis)
$Na + L \rightleftharpoons NaL$	12.94	12.94 ± 0.02	complex formation
$NaL + Na \rightleftharpoons Na_2L$	6.88	6.87 ± 0.01	complex formation

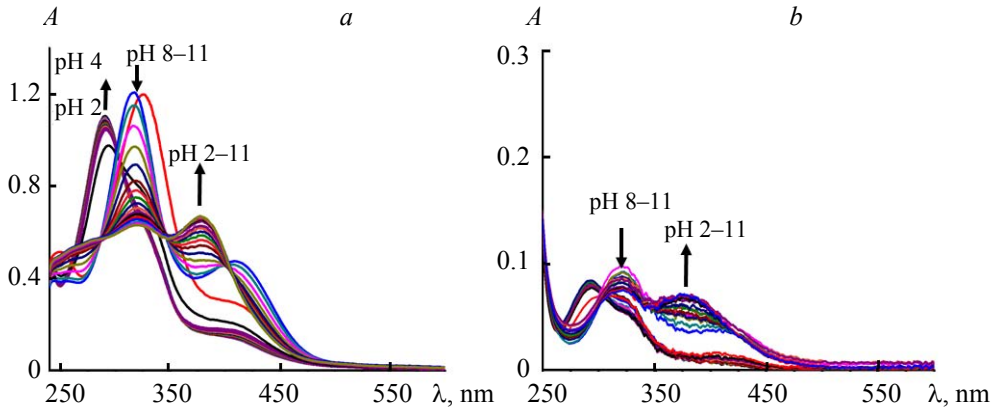

Fig. 8. Experimental electronic spectra of the (a) ligand MEP and (b) ligand with Na(I) ion in 1:2 ratios with increasing pH.

In the spectrometric method, the formation constant of the Na(I)-MEP complex was also calculated by using the HypSpec program. The model gave the best fits when NaL and Na_2L species were considered in the calculation. The values obtained are 12.94 M^{-1} and 6.88 M^{-2}, respectively, and are given in Table 4, which shows good agreement with each other and also with the association constant for Na_2L complex formation as obtained by fluorimetric method (Table 2). The fluorimetric data, however, did not detect any 1:1 complex formation (NaL), which may be due to the absence of any significant changes in the fluorescence spectra of both types of complexes. The absorption spectra of the ligand in the presence of Na(I) with increasing pH is shown in Fig. 8b. The formation of the Na_2L complex can be attributed to the trapping of sodium ions into two pseudo-cavities created due to the interaction of two O atoms and one N atom of ortho –OH, amide, and imine groups, respectively, as shown in Fig. 6. These structures were obtained from the DFT optimized structures of the ligand and the complex.

Conclusions. A novel dipodal fluorescent chelator MEP with a malonate platform carrying pendants of pyrogallol as binding units and ethylenediamine as a spacer was developed. The photophysical studies of the ligand explored its high selectivity for Na(I) metal ions over a wide range of important metal ions by showing a prominent enhancement in fluorescence emission at room temperature. The probe acted efficiently in sensing Na(I) with a minimum detection limit of 1.98×10^{-4} in DMSO medium. Pre-organization of the flexible pendant arms, suitable cavity size, and availability of polyfunctional donor sites in the structural framework promote strong ligand-metal interaction, as indicated by the high formation constant of the complex, 7.7×10^6 M^{-2} (logβ = 6.88). The potentiometric and spectrophotometric investigation established the formation of two species, NaL and Na_2L, with stability constants (logβ) 12.94 and 6.88, respectively. The molecular modeling studies at the DFT level suggest that the stability of the complexes is due to trapping of the two metal ions in the two cavities created by interaction of the ortho –OH, amide –O, and imine –N atoms.

The Na-O and Na-N bond distances are comparable with that of Na-aza-crown ether complexes. The excellent binding abilities and fluorescence behavior enable the ligand MEP to be employed for efficient detection and measurements of Na(I) ions in environmental samples like urine, sweat, etc. There is also ample scope for exploring the potential use of the newly developed dipodal fluorescent probe, which can serve as a promising tool for determining an important parameter, the Na(I) level, for industrial applications.

Acknowledgments. The authors acknowledge financial assistance from MHRD and are thankful to SAIF, PU, Chandigarh for providing instrument facilities.

REFERENCES

1. A. P. de Silva, H. Q. Gunaratne, T. Gunnlaugsson, A. J. Huxley, C. P. McCoy, J. T. Rademacher, T. E. Rice, *Chem. Rev*., **97**, 1515–1566 (1997).
2. J. F. Callan, A. P. de Silva, D. C. Magri, *Tetrahedron*, **61**, 8551–8588 (2005).
3. A. Coskun, M. Banaszak, R. D. Astumian, J. F. Stoddart, B. A. Grzybowski, *Chem. Soc. Rev*., **41**, 19–30 (2012).
4. R. Akbar, M. Baral, B. K. Kanungo, *J. Coord. Chem*., **71**, N 1, 135–154 (2018).
5. M. Baral, A. Gupta, R. Akbar, B. K. Kanungo, *J. Appl. Chem*., **2016**, 3757418/1–3757418/10 (2016).
6. M. Baral, A. Gupta, B. K. Kanungo, *Spectrochim. Acta A*, **162**, 6–15 (2016).
7. M. Burnier, *Sodium in Health and Disease*, Informa Healthcare, New York (2008).
8. *The Na^+, K^+ Pump, Part B: Cellular Aspects*, Eds. J. C. Skou, J. G. Norby, A. B. Maunsbach, M. Esmann, A. R. Liss, Wiley, New York (1998).
9. E. Murphy, D. A. Eisner, *Circ. Res*., **104**, 292 (2009).
10. D. M. Bers, W. H. Barry, S. Despa, *Cardiovasc. Res*., **57**, 897 (2003).
11. T. R. Harring, N. S. Deal, D. C. Kuo, *Emerg. Med. Clin. North Am*., **32**, 379–401 (2014).
12. Z. J. Twardowski, *Hemodial. Int*., **12**, 412–425 (2008).
13. A. Minta, R. Y. Tsien, *J. Biol. Chem*., **264**, 19449 (1989).
14. *Chemosensors of Ion and Molecule Recognition; NATO ASI Series,* Eds. J. P. Desvergne, A. W. Czarnik, Kluwer Academic, Dordrecht, The Netherlands (1996).
15. O. S. Wolfbeis, *Fiber Optic Chemical Sensors and Biosensors*, **II**, CRC Press, Boca Raton, FL (1991).
16. P. Gans, A. Sabatini, A. Vacca, *Talanta*, **43**, 1739–1753 (1996).
17. P. Gans, A. Sabatini, A. Vacca, *Ann. Chim. (Rome)*, **89**, 45–49 (1999).
18. S. K. Sahoo, S. E. Muthu, M. Baral, B. K. Kanungo, *Spectrochim. Acta A*, **63**, 574 (2006).
19. L. J. Bellamy, *The Infra-red Spectra of Complex Molecules*, 3rd ed., Chapman and Hall Ltd., London (1975).
20. R. M. Silverstein, G. C. Bassler, T. C. Morrill, *Spectrometric Identification of Organic Compounds*, 4th ed., Wiley, New York (1981).
21. Y. K. Tsui, S. Devaraj, Y. P. Yen, *Sens. Actuat. B: Chem*., **161**, 510–519 (2012).
22. A. P. de Silva, H. Q. N. Gunaratne, J. L. Habib-Jiwan, C. P. McCoy, T. E. Rice, J. P. Soumillion, *Angew. Chem., Int. Ed. Engl*., **34**, 1728–1731 (1995).
23. H. Huarui, M. A. Mortellaro, M. J. P. Leiner, S. T. Young, R. J. Fraatz, J. K. Tusa, *Anal. Chem*., **75**, 549–555 (2003).
24. Graham R. C. Hamilton, Suban K. Sahoo, Sukanta Kamila, Narinder Singh, Navneet Kaur, Barry W. Hyland, John F. Callan, *Chem Soc Rev*., **7**, N 44(13), 4415–4432 (2015).
25. Y. M. Poronik, G. Clermont, M. Blanchard-Desce, D. T. Gryko, *J. Org. Chem*., **78**, N 23, 11721–11732 (2013).
26. Kundan Tayade, G. Krishna Chaitanya, Jasminder Singh, Narinder Singh, Sopan Ingle, Sanjay Attarde, Anil Kuwar, *J. Lumin*., **154**, 68–73 (2014).
27. M. Everett, A. Jolleys, W. Levason, D. Pugh, G. Reid, *Chem. Commun*., **50**, 5843–5846 (2014).
28. H. A. Benesi, J. H. Hilderbrand, *J. Am. Chem. Soc*., **71**, 2703–2704 (1949).
29. G. Kaur, N. Kaur, *Sens Actuat. B: Chem*., **265**, 134–141 (2018).
30. W. Caetano, M. Tabak, *J. Colloid Interface Sci*., **225**, 69–81 (2000).
31. Y.-J. Hua, Y. Liua, T.-Q. Sunb, A.-M. Bai, J.-Q. Lu, Z.-B. Pi, *Int. J. Biol. Macromol.*, **39**, 280–285 (2006).
32. H. W. Jun, L. A. Luzzi, P. L. Hsu, *J. Pharm. Sci*., **61**, N 11, 1835–1837 (1972).
33. X. Mei, C. Wolf, *J. Am. Chem. Soc*., **126**, 14736–14737 (2004).
34. J. R. Lakowicz, *Principles of Fluorescence Spectroscopy*, 3rd ed., Springer, Berlin (2006).